THE JOURNAL OF PHYSICAL CHEMISTRY C

Article

pubs.acs.org/JPCC

# Enhanced Charge Transfer Doping Efficiency in J-Aggregate Poly(3-hexylthiophene) Nanofibers

Jian Gao, Benjamin W. Stein, Alan K. Thomas, Jose A. Garcia, Jing Yang, Martin L. Kirk, and John K. Grey*

Department of Chemistry and Chemical Biology, University of New Mexico, Albuquerque, New Mexico 87131, United States

Supporting Information

**ABSTRACT:** Charge transfer doping efficiencies of $\pi$-stacked poly(3-hexylthiophene) (P3HT) aggregate nanofibers are studied using spectroscopic and electron microscopy probes. Solution dispersions of self-assembled P3HT nanofibers are doped in the ground electronic state by adding varying amounts (w/w%) of the strong charge transfer dopant 2,3,5,6-tetrafluoro-7,7,8,8-tetracyanoquinodimethane ($F_4$-TCNQ). Careful control of self-assembly conditions allows us to select either the H- and J-aggregate limiting forms, which differ primarily in the degree of purity (i.e., molecular weight fractionation) and nanomorphology. Electron paramagnetic resonance (EPR), electronic absorption, and Raman spectroscopy of $F_4$-$TCNQ^-$:$P3HT^+$ species are then used to track doping efficiency with dopant loading. J-aggregate nanofibers exhibit over an order of magnitude larger doping efficiencies than polymorphic H-aggregate nanofibers. The higher purity and order of the former promote intrachain polaron delocalization whereas disorder arising from greater molecular weight polydispersity in the latter instead lead to polaron localization resulting in charge transfer complex formation. Interestingly, J-aggregate nanofiber EPR signals decrease significantly after ~25% $F_4$-TCNQ loading which we attribute to increased antiferromagnetic coupling between delocalized hole polarons on neighboring P3HT chains leading to spinless interchain bipolarons. Raman spectra excited on resonance with NIR $F_4$-$TCNQ^-$:$P3HT^+$ absorption transitions also reveal quinoid distortions of the P3HT backbone in J-aggregates. We propose that self-assembly approaches to control aggregate packing and purity can potentially be harnessed to achieve long-range, anisotropic charge transport with minimal losses.

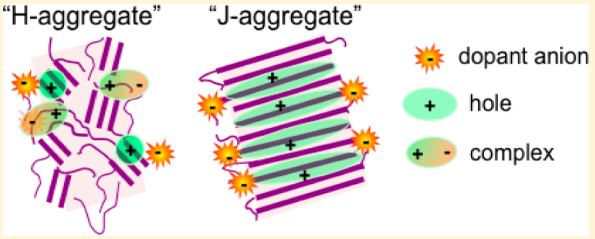




## INTRODUCTION

Ground state charge transfer hole (i.e., p-type) doping of conjugated polymers is a simple, but effective, strategy for increasing conductivities and improving the overall performance of polymer-based optoelectronic devices.[1−7] Traditionally, polymers are doped electrochemically or upon exposure to mineral acids, but more recently, small molecule charge transfer dopants have emerged as dopants of choice. These molecules are typically combined with polymers dissolved in common organic solvents prior to deposition of thin films. Solution polymer−dopant encounter interactions result in quantitative charge transfer if sufficient offset exists between the polymer HOMO and dopant LUMO levels.[8−10] However, charge transfer doping efficiencies (i.e., free carrier levels) of thin films prepared from these solutions are often much lower than expected based on dopant loading.[11,12] Recent efforts have been directed toward understanding the origins of these discrepancies and the general consensus points to either partial charge transfer or formation of charge transfer complexes.[8,11,13−15] However, the structural and morphological origins of the discrepancies between doping efficiency (i.e., free charge carrier densities) and dopant loading are less apparent. We now seek a new understanding of molecular structural and morphological factors regulating polymer−dopant interactions and charge transfer doping efficiency by studying a benchmark polymer and charge transfer dopant system.

Poly(3-hexylthiophene) (P3HT) is an archetype conjugated polymer and can be doped in its ground electronic state by the strong acceptor 2,3,5,6-tetrafluoro-7,7,8,8-tetracyanoquinodimethane ($F_4$-TCNQ).[8,11,12,16−21] P3HT is also known to form ordered $\pi$-stacked aggregates[22] which facilitate efficient multidimensional charge and energy transport leading to improved material performance.[23,24] Spectroscopic probes (i.e., electronic absorption and Raman spectroscopies) are the most effective for both quantifying the amount of aggregation as well as the nature of exciton coupling within these structures, which is advantageous for doping studies since measurements can be performed in either the solution or solid phase. It is generally accepted that the high electron affinity of $F_4$-TCNQ (~5.2 eV) compared to the reported ionization potential of P3HT (~4.8 eV) results in quantitative charge transfer interactions[8] regardless of the polymer aggregation state. However, ordered (aggregated) and disordered (amorphous) P3HT chains exhibit different electronic properties (i.e., optical band gap, charge mobility, etc.), suggesting that polymer−dopant interactions and doping efficiencies should likewise also

**Received:** May 31, 2015
**Published:** June 24, 2015




DOI: 10.1021/acs.jpcc.5b05191
J. Phys. Chem. C 2015, 119, 16396−16402

be different. In an earlier study, we investigated the effect of P3HT regioregularity—which determines the conformational attributes of individual chains as well as the ability to form aggregates—on doping efficiency in dilute solution.[20] Highly regioregular P3HT (>99% head-to-tail) samples showed efficient doping that we attributed to their ability to adopt relatively ordered (viz. planar) conformations in aggregates, resulting in intrachain hole delocalization. Conversely, regiorandom P3HT exists entirely in disordered (twisted) conformations causing charge localization and the formation of tightly bound charge transfer complexes, resulting in poor doping efficiency by trapping mobile charge carriers.[20] Although studies of nascent solution phase P3HT/$F_4$-TCNQ interactions offer additional insights into structural factors affecting doping efficiency, a significant gap still remains in understanding and reconciling observed doping efficiencies with morphologies more closely representing those encountered in thin films. We now use polymer aggregates as platforms for further examining the delicate interplay between nanomorphology and aggregate purity on charge injection and interactions upon doping with small molecule charge transfer additives.

Solution dispersions of P3HT aggregate nanofibers are prepared using self-assembly techniques to direct chain packing order and nanomorphology. By controlling aggregate self-assembly conditions via solvent and temperature, aggregate polydispersity and packing order can be regulated which enables tunability of exciton coupling. For example, P3HT is sparingly soluble in anisole and aggregate nanofibers form rapidly upon cooling when heated up to the solvent boiling temperature. Optical spectra of these structures resemble characteristic H-aggregates arising from lower intrachain order localizes excitons leading to dominant interchain coupling. On the other hand, slow cooling of P3HT dissolved in toluene solutions results in highly fractionated aggregates with high intrachain order and few stacking faults. Corresponding optical spectra reveal dominant intrachain exciton coupling or J-aggregate behavior. These H- and J-type P3HT aggregates therefore allow for detailed investigations of charge injection following polymer−dopant contact interactions in solution as well as interactions between carriers of the same and opposite sign. For this purpose, we employ electronic absorption, resonance Raman, and electron paramagnetic resonance (EPR) spectroscopy with doped nanofibers in dilute solution, which avoids potential complications from morphological heterogeneity found in thin films since the nanofiber morphology remains fixed.

Despite seemingly subtle differences in structure and morphology between both nanofiber types, vastly different doping responses are observed upon addition of $F_4$-TCNQ to solution nanofiber dispersions. For example, H-type nanofibers display maximum doping levels (i.e., $F_4$-$TCNQ^-$:$P3HT^+$ EPR spin densities and absorption signatures) at ∼7% (w/w) $F_4$-TCNQ loading which gradually decrease at larger loadings, similar to P3HT thin films. J-type aggregate nanofibers show over an order of magnitude larger EPR signal strength at maximum dopant loadings of ∼25% w/w. Corresponding Raman spectra generated on resonance with $F_4$-$TCNQ^-$:$P3HT^+$ absorption bands show evidence of P3HT quinoid distortions in J-type nanofibers, indicating efficient intrachain hole polaron delocalization.[25−27] Interestingly, integrated EPR spin densities decrease significantly for $F_4$-TCNQ loadings >25% in J-aggregates. We attribute this effect to antiferromagnetic exchange coupling between hole polaron spins on neighboring π-stacked P3HT chains resulting in interchain, spinless bipolarons.[28,29] However, these interchain polaron interactions do not appear to significantly perturb one photon absorption selection rules governing the absorption strength of $F_4$-$TCNQ^-$:$P3HT^+$ species, which continues to increase over the same loading range. The results demonstrate the importance of nanomorphology and purity of aggregates in determining doping efficiency that are not readily discernible from studies of conventional thin films.

## EXPERIMENTAL SECTION

**Sample Preparation.** Regioregular P3HT ($M_n$ = 65 kDa, PDI = 1.3) was obtained from Sigma-Aldrich and used without further purification. Anisole and toluene are used as solvents for fabricating H-type and J-type P3HT nanofibers, respectively, following procedures reported previously.[30,31] $F_4$-TCNQ (Sigma-Aldrich) was dissolved in both anisole and toluene solvents at a concentration of 1 mg/mL and then stirred for ∼8 h in a dry nitrogen environment. $F_4$-TCNQ solutions were added to P3HT nanofiber solution dispersions, which were held constant for all dopant loadings.

**Spectroscopic Instrumentation.** Raman spectra were also recorded on the same samples using a dispersive spectrometer (Thermo Fisher Scientific) with NIR excitation (785 nm). EPR spectra of solution nanofiber dispersions were collected at both X-band (9.4 GHz) and Q-band (∼36 GHz) frequencies using a dedicated Bruker EMX spectrometer with associated Bruker magnet control electronics and microwave bridges. A microwave power of 2.11 mW (20 dB attenuation) was used for all experiments. Spectra were collected at 298 and 5 K in the dark using an Oxford Instruments liquid helium flow cryostat. EPR measurements were also performed in the $g \sim 4$ region to determine if half-field transitions from triplet states were present over the range of dopant loadings studied. Electronic absorption spectra were collected at 298 K using a Hitachi U-3501 UV−vis−NIR dual-beam spectrometer capable of scanning a wavelength region between 185 and 3200 nm. The electronic absorption spectra of P3HT nanofiber/$F_4$-TCNQ solution dispersions were collected using microcuvettes in order to avoid the potential Beer's law deviations and associated nonlinearity resulting from the large nanofiber absorptivities.

## RESULTS AND DISCUSSION

Aggregate electronic properties are assessed using the weakly coupled HJ aggregate model developed by Spano and coworkers[32,33] which relates the strength of both intra- and interchain exciton coupling to aggregate order. Previous structural studies of both aggregate types reveal similar P3HT π-stacking distances[31] although the effects of more subtle chain packing order are obtained from spectroscopy. Figure 1 shows representative electronic absorption spectra of (a) J-type and (b) H-type P3HT nanofiber solution dispersions as a function of $F_4$-TCNQ loading. Optical densities were <1 for all samples, and sample response varied linearly with concentration. Upon addition of dopant, both nanofiber types display a characteristic increase in a NIR transition absorbance with partially resolved vibronic structure corresponding to overlapping absorption transitions of $F_4$-$TCNQ^-$ and $P3HT^+$.[24,34] This assignment was confirmed by doping $F_4$-TCNQ and P3HT separately with ferrocene and 2,3-dichloro-5,6-dicyano-1,4-quinone (DDQ),


DOI: 10.1021/acs.jpcc.5b05191
J. Phys. Chem. C 2015, 119, 16396−16402

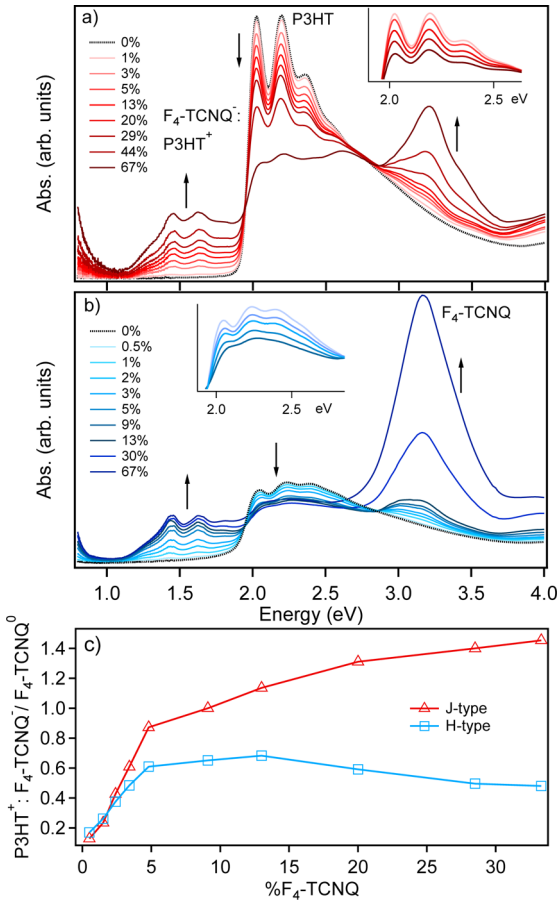


**Figure 1.** Electronic absorption spectra of (a) J-aggregate type and (b) H-aggregate type P3HT nanofibers dispersed in toluene and anisole solutions, respectively, and doped with $F_4$-TCNQ. Absorption signatures of pristine and charged P3HT and $F_4$-TCNQ species are indicated. Insets: vibronic distributions of pristine P3HT aggregates for selected dopant loadings (0.5–20%). (c) Comparison of $F_4$-TCNQ$^-$:P3HT$^+$/$F_4$-TCNQ absorption ratios for H- and J-type P3HT nanofibers up to 30% loading.

respectively (see Figure S1, Supporting Information). We found no evidence of $F_4$-TCNQ$^{2-}$ species[34] although these may, if present, overlap with neutral P3HT aggregate absorption line shapes. Absorption transitions of neutral $F_4$-TCNQ are also apparent in the near-UV spectral region ($E_{max}$ ~ 3.25 eV) and become more prominent presumably when accessible interaction sites become filled. The pristine P3HT aggregate $\pi$–$\pi^*$ absorption region is also highlighted in the insets for each NF type (Figure 1, insets) to illustrate how doping impacts exciton coupling characteristics. J-type nanofibers show a distinct change in the vibronic distributions where the 0–0 transition decreases relative to the 0–1 and other vibronic transitions for larger dopant loading in addition to slight spectral broadening. This effect suggests agglomeration,[30,35] which is known to perturb intrachain order causing a loss of J-aggregate character. Conversely, H-type nanofibers only display increased broadening with dopant loading. No significant shifting of P3HT-centered transitions occurs in nanofiber spectra, indicating that the native structure and packing are preserved, which we confirm with fluorescence emission spectroscopy (see Figure S2, Supporting Information) and TEM imaging (*vide infra*).

Despite the overlapping nature of P3HT$^+$ and $F_4$-TCNQ$^-$ absorption signatures, it is still possible to compare dopant loading-dependent trends to the observed doping efficiency. Ratios of the integrated absorbance of $F_4$-TCNQ$^-$:P3HT$^+$ species with the neutral, uncomplexed $F_4$-TCNQ absorption transition ($F_4$-TCNQ$^-$:P3HT$^+$/$F_4$-TCNQ) appearing on the blue edge of the neutral P3HT aggregate line shape were measured as a function of $F_4$-TCNQ loading and displayed in Figure 1c. Because the amounts of P3HT differ in both nanofiber types due to fractionation in J-type structures, absorption spectra were normalized at the lowest loading (~0.5%) by applying a multiplicative scaling factor. Linear increases in the amounts of $F_4$-TCNQ$^-$:P3HT$^+$ are observed from ~0 up to ~5% for both nanofiber types. After this level, H-type nanofibers show smaller increases up to ~10% loading and then decrease gradually as the amount of uncomplexed $F_4$-TCNQ increases without concomitant increase in the concentration of the $F_4$-TCNQ$^-$:P3HT$^+$ absorption strength. J-type nanofibers show much larger increases in $F_4$-TCNQ$^-$:P3HT$^+$/$F_4$-TCNQ absorption ratios and continue to increase as the dopant loading approaches the maximum amount used in this study (~35%).

Alternate views of doping efficiencies can be obtained from EPR spectroscopy, which directly probes the environments of unpaired spin centers on donor and acceptor sites. Figure 2 shows representative X-band (9.38 GHz) EPR spectra of J-type and H-type nanofiber dispersions (Figures 2a and 2b, respectively) with $F_4$-TCNQ loadings in the ~0.5–30% range. Pristine P3HT nanofiber solution dispersions display no EPR signals, demonstrating that intrinsic charge carrier levels in the P3HT ground electronic state are negligible, as expected. Even for relatively small $F_4$-TCNQ levels (<1%) a characteristic EPR signature emerges for both nanofiber types indicating doping of P3HT chains in both aggregate types. The *g*-values for both nanofiber types ($g$ ~ 2.003) are close to the free electron value (2.0023), indicating the signal is monoradical in nature with no apparent anisotropy or hyperfine structure. However, similar to absorption spectra trends in Figure 1, $F_4$-TCNQ$^-$ and P3HT$^+$ resonances overlap, leading to the appearance of a single unpaired spin. This was confirmed by cursory X-band EPR studies with DDQ as the dopant that reveal two distinct resonances (see Figure S3, Supporting Information).

EPR spectra (i.e., $F_4$-TCNQ$^-$:P3HT$^+$ spins) were next double integrated and plotted as a function of dopant loading over the entire range studied and shown in Figure 2c. We applied the same multiplicative scaling factor to integrated EPR intensities in order to compare to doping responses in electronic absorption spectra (Figure 1). Similar trends are observed in the low doping regime (<5%) as both nanofibers show linear increases in doubly integrated EPR signal with $F_4$-TCNQ loading. The H-type EPR trends in Figure 2c are nearly identical to the $F_4$-TCNQ$^-$:P3HT$^+$/$F_4$-TCNQ absorption ratios in Figure 1c where values reach a maximum around ~7% loading then decrease gradually for larger loadings. J-type nanofibers show a larger and linear increase in EPR intensity, consistent with a larger amount of unpaired spins, up to ~25% loading before decreasing sharply at higher loadings. Interestingly, this trend contradicts observed behaviors from electronic absorption spectra that show a linear increase in the ionized forms as loadings increase. The origins for the apparent loss of spin densities at higher dopant loading in J-aggregate nanofibers are considered in detail below.


DOI: 10.1021/acs.jpcc.5b05191
J. Phys. Chem. C 2015, 119, 16396–16402

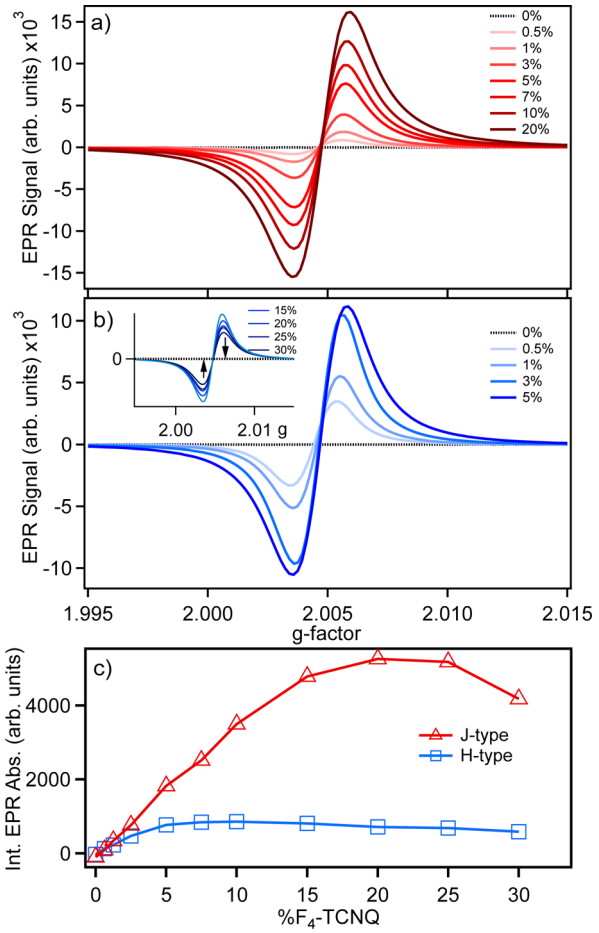


**Figure 2.** Representative X-band EPR spectra of (a) J-type and (b) H-type P3HT nanofibers with varying $F_4$-TCNQ loading. Spectra are shown for H-type nanofiber EPR signals noticeably decrease with loadings >10% and are highlighted in the inset. (c) Integrated EPR signal for H- and J-type P3HT nanofibers measured up to 30% dopant loading at 300 K.

Because of the overlapping nature of unpaired $F_4$-TCNQ$^-$ and P3HT$^+$ spins, EPR spectra of doped H- and J-type P3HT nanofibers were measured using Q-band frequencies (~36 GHz) to determine if these species could be resolved separately. Figure 3 shows Q-band EPR spectra measured at 5 K for H- and J-type nanofibers at the same $F_4$-TCNQ loading (5%). Line widths are ~0.8 mT for H-type and ~0.5 mT for J-type with *g*-values of 2.004 and 2.005, respectively. Room temperature Q-band EPR spectra were also measured with similar features albeit lower signal-to-noise ratios (see Figure S4, Supporting Information). The changes in *g*-value and line shape of the dominant contributions to the Q-band spectra reflect the environment of the unpaired electron(s), and these are subtly but clearly different for each nanofiber type. For example, the larger *g*-value observed for J-type nanofibers indicates an increase in spin−orbit coupling for these doped structures. A weakly resolved resonance near $g \sim 2.0025$ (indicated by the arrow in Figure 3) is also apparent in J-type nanofibers probably corresponding to small amounts of radical impurities and not from either $F_4$-TCNQ$^-$:P3HT$^+$ species.

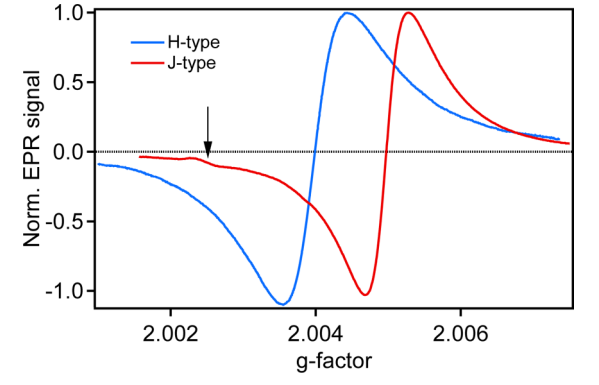


**Figure 3.** 5K Q-band EPR spectra of doped H- and J-type nanofibers at 5% $F_4$-TCNQ loading.

The differences in doping response of H- and J-aggregate P3HT nanofibers to varying $F_4$-TCNQ loading can largely be attributed to differences in both the aggregate purity and nanomorphology. We do not attempt to undertake structural characterization studies in the dilute nanofiber dispersions as a function of dopant loading; however, correlations between doping efficiency and aggregate morphology can be obtained from their established exciton coupling characteristics. The dominant intrachain character in J-type nanofibers suggests that injected hole polarons should similarly be able to delocalize along P3HT backbones, thus resulting in successful doping. The high intrachain order and packing integrity of these structures also minimize trapping and collapse into charge transfer complexes that reduce doping efficiency. Conversely, H-aggregate P3HT nanofiber morphologies more closely resemble thin films with smaller, less-ordered aggregate domains bordered by amorphous regions. This situation is encountered due to the inclusive nature of nanofiber assembly where all molecular weight fractions are incorporated in the nanofiber, unlike the highly fractionated J-aggregates. Greater disorder localizes polarons leading to charge transfer complexes in the presence of $F_4$-TCNQ, which is consistent with a gradual decrease of free charge carrier densities. It is important to stress that while electronic spectroscopies such as absorption and EPR are useful for understanding the fates of injected charges, the response of the P3HT skeletal framework in both aggregate nanofibers is less apparent. We now turn to Raman spectroscopy, which offers additional perspectives of structural changes in response to doping in H- and J-type nanofibers.

Unlike electronic absorption and EPR spectroscopic metrics of doping efficiency in P3HT aggregates, the narrower line widths of specific vibrational transitions in Raman spectra avoid complications from broad and overlapping line shapes, making their interpretation potentially less ambiguous. Figure 4 displays Raman spectra of H- and J-type P3HT nanofibers generated using excitation energies that are off resonance with the neutral P3HT aggregate absorption transitions ($\lambda_{exc}$ = 785 nm, 1.58 eV). However, this excitation wavelength is resonant with the NIR absorption transitions of $F_4$-TCNQ$^-$ and P3HT$^+$ species. Similar to our EPR and absorption results, Raman trends from both nanofiber types reveal markedly different responses and spectral signatures for J-type nanofibers (Figure 4a) compared to H-type nanofibers (Figure 4b) over the same dopant loading ranges. Raman bands associated with $F_4$-TCNQ$^-$ are apparent in the ~1650−1700 cm$^{-1}$ range for both nanofibers but are more intense for J-type nanofibers, consistent with absorption and EPR trends shown in Figures 1−3. Turning to the CC stretching region of the P3HT backbone region (~1300−1600 cm$^{-1}$), J-type nanofibers show more drastic changes than H-type nanofibers for comparable


DOI: 10.1021/acs.jpcc.5b05191
J. Phys. Chem. C 2015, 119, 16396−16402

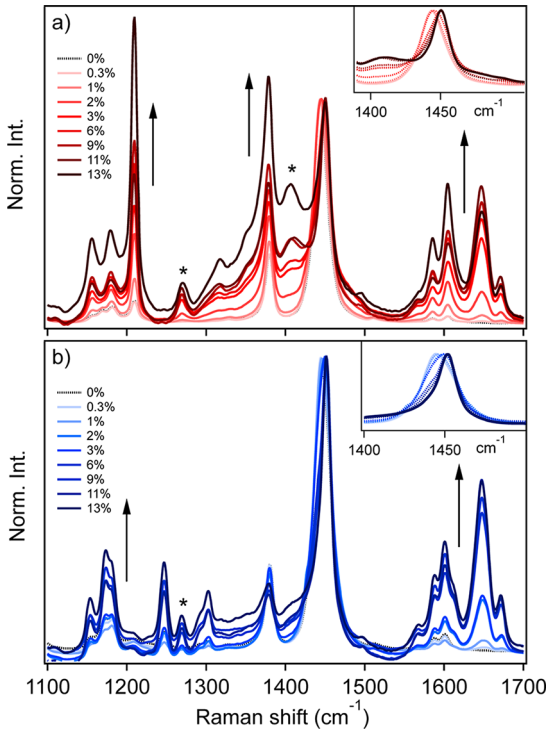


**Figure 4.** Raman spectra of (a) J-type and (b) H-type P3HT nanofiber dispersions with varying $F_4$-TCNQ loadings. The excitation wavelength ($\lambda_{exc}$ = 785 nm) is resonant with the NIR absorption line shape of $F_4$-$TCNQ^-$:$P3HT^+$ denoted in Figure 1. Asterisks denote a new transition that increases with $F_4$-TCNQ loading in both nanofibers.

dopant loadings. Namely, large increases in the relative intensities of the nominal C−C stretch (~1390 $cm^{-1}$) in addition to the inter-ring breathing mode at ~1212 $cm^{-1}$ are observed with increased loading. C═C symmetric stretching bands of both P3HT NF types also blue-shifted by ~7 $cm^{-1}$ (Figure 4 insets) up to the largest dopant loading. H-type nanofiber Raman spectra are not largely perturbed in the P3HT backbone region with addition of $F_4$-TCNQ and mainly show intensity increases of vibrations localized on $F_4$-TCNQ in addition to some lower frequency P3HT centered vibrations (~1100−1300 $cm^{-1}$).

Previous Raman spectroscopic studies of heavy doping in polythiophenes reported the tendency of the backbone to undergo a quinoid distortion from the dominant benzoid (aromatic) form in neutral molecules.[25,36] Comparison of doped J-type nanofibers in Figure 4a with Raman spectral signatures of polythiophene quinoid species suggests that P3HT chains in these nanofiber structures more readily convert to the quinoid form upon doping. These structural distortions are conspicuously absent in H-type nanofibers consistent with greater localization of injected holes and collapse into bound charge transfer complexes as dopant loadings increase.[37] The larger doping efficiencies and pronounced quinoid distortions in J-type nanofibers (e.g., intensity redistributions of the P3HT C═C and C—C stretches) suggest metallic character, similar to reports involving related doped polymer systems.[38]

A new transition also becomes resolved in doped H- and J-type Raman spectra located at ~1270 $cm^{-1}$ and increases in response to $F_4$-TCNQ addition. Previous DFT Raman simulations of oligothiophenes indicate that transitions in this region have symmetric inter-ring stretching character that increase in activity because of intermolecular charge transfer interactions.[21] Although this transition may potentially serve as a spectroscopic marker of doping efficiency between both types of nanofibers, pronounced decreases in signal-to-noise ratios and increased broadening were observed beyond ~15% loading. These aspects, along with the lack of suitable intensity standard, preclude detailed comparisons with established from EPR and absorption spectra.

The spectroscopic data presented in Figures 1−4 show distinct dependences on doping responses with P3HT nanofiber order and morphology. However, these techniques are less sensitive to changes in larger scale features incurred from doping (e.g., nanofiber interactions). Previous structural studies of doped P3HT thin films also found evidence for a new phase which may explain changes in vibronic distributions and broadening in absorption spectra. We perform TEM imaging of pristine (a, c) and doped (b, d) J- and H-type P3HT nanofibers, respectively, to assess if nanofiber structural integrity is altered due to doping. These images are shown in Figure 5, and generally, addition of $F_4$-TCNQ causes nanofibers

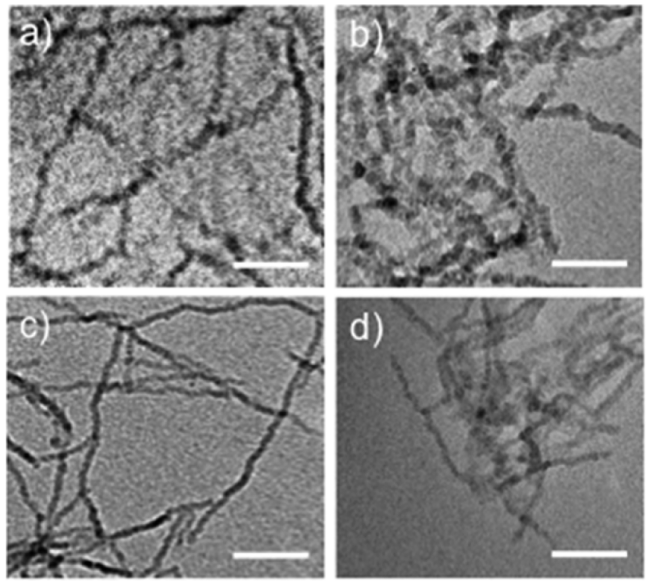


**Figure 5.** TEM images of pristine and doped (5% $F_4$-TCNQ) J-type (a, b) and H-type (c, d) nanofibers, respectively. Scale bar = 200 nm.

to agglomerate probably from doping-induced formation of charge transfer salts. However, nanofiber structural qualities and aspect ratios for both types are not significantly affected although agglomeration likely disrupts intra- and interchain order. This is particularly evident in J-type nanofibers (Figure 1a, inset) that tend to become more H-aggregate-like (i.e., 0−0/0−1 vibronic strengths <1 and broader line widths) at larger dopant loadings. Similar effects were also observed upon subjecting these structures to high external pressures that partially restores interchain exciton character due to minor structural perturbations on the periphery of the structure that disrupt intrachain order.[35]

**Correlating Conformational and Packing Order to Doping Efficiency and Polaron Interactions.** Our results indicate that the significantly larger polaron densities (doping efficiencies) and quinoidal character of J-type P3HT nanofibers originates from higher intrachain order and chain packing integrity that promotes polaron delocalization along the P3HT backbone. However, decreases in EPR intensities at loadings


DOI: 10.1021/acs.jpcc.5b05191
J. Phys. Chem. C 2015, 119, 16396−16402

>25%, despite continuously increasing $F_4$-TCNQ$^-$:P3HT$^+$ absorption strengths, indicate either suppressed spin relaxation rates or magnetic exchange interactions between hole polaron spins in this doping regime. The loss of polaron spin density at these larger loadings potentially limits the ultimate attainable doping levels, and we now consider the role of P3HT chain ordering on interactions between injected hole polarons.

We propose that antiferromagnetic exchange coupling between hole polarons on neighboring chains in the J-aggregate $\pi$-stack (i.e., superexchange or direct exchange coupling) is chiefly responsible for observed decreases in EPR intensities at high loadings.[39,40] These exchange interactions give rise to an interchain spinless bipolaron state, similar to earlier findings in heavily doped polymer and oligomer films.[28,41−43] At low dopant loadings, the probability of hole spins interacting on J-type P3HT chains is very small due to their delocalized nature and small interchain coupling. At higher dopant loading, holes may begin to interact on adjacent chains,[44] but the linear increase of $F_4$-TCNQ$^-$ and P3HT$^+$ absorption strength in the same dopant loading range suggests these antiferromagnetic interactions do not significantly alter the one-photon electronic absorption selection rules. Another possibility is that double ionization of single chains within these aggregates occurs resulting in intrachain bipolaron states.[45] If this were the case, electronic absorption line shapes would deviate substantially from simple linear combinations of neutral and singly ionized forms of polymer and dopant observed in Figure 1.

Doping responses from P3HT H-aggregate nanofibers display only gradual decreases in both EPR and absorption that is consistent with the majority of injected holes trapped in charge transfer complexes. Similar behaviors have been reported in doped P3HT thin films and conductivity studies revealed that only ∼5% of injected holes contribute to electrical conduction. Aggregated regions in both P3HT H-type nanofiber and thin films are generally smaller due to the presence of interpenetrating amorphous chains that cause packing faults, thus diminishing intrachain order. As a result polaron migration lengths are smaller, leading to increased trapping in charge transfer complexes in addition to a smaller amount of suitable and accessible doping sites.

## CONCLUSIONS

The results presented herein offer new views of the delicate interplay between polymer conformational and packing ordering and obtainable doping efficiencies. Most notably, current doping models have not explicitly considered the roles of these delicate structural factors on determining polymer-dopant and polaron interactions. However, the integer charge transfer doping model put forth recently by Pingel and Neher provides a basis for explaining observed trends in Figures 1−4.[12] For example, if the injected polymer hole polaron can escape the Coulombic attraction with the ionized dopant, increased free carrier levels and conductivities are observed. Based on our present and previously reported findings,[46] polymer chains with high intrachain order promote exciton and polaron intrachain delocalization which is essential for producing mobile charges and increasing conductivity. Otherwise, conformational and packing disorder (i.e., torsional distortions, packing defects, and ordered−disordered domain boundaries) localizes injected holes leading to bound charge transfer complexes that do not contribute to increased conductivity. These disorder effects are minimized in J-type nanofibers due to molecular weight fractionation during aggregate assembly, resulting in aggregates of greater purity and crystallinity. Injected holes are then able to escape Coulombic attraction with ionized dopants leading to free charge carriers. Conversely, an appreciable amorphous fraction leads to underdeveloped aggregates (i.e., H-aggregates) with lower intrachain order that limits charge mobility and suitable dopant interaction sites.

Overall, we have shown that self-assembly approaches can be effectively utilized to tune doping efficiencies by controlling aggregate order and morphology. These nanofiber platforms also help bridge the gap in understanding polymer-dopant and polaron interactions that are usually obscured in conventional doping studies due to the evolution of complex morphological features during film deposition (e.g., spin-casting) following addition of dopants in solution. We have further demonstrated that the formation of spinless bipolaron-like states observed in highly doped J-aggregate nanofibers via interchain antiferromagnetic coupling is the limiting factor for further maximizing doping efficiencies in these systems. Lastly, the larger doping efficiencies found in J-aggregates may have implications for achieving efficient, long-range charge transport with minimal losses due to preservation of their structures over a large doping range.[38,47]

## ASSOCIATED CONTENT

### Supporting Information

Optical absorption of doped P3HT and $F_4$-TCNQ, fluorescence emission spectra of doped H- and J-type P3HT nanofibers, EPR spectra of P3HT doped with DDQ, room temperature Q-band EPR spectra of doped P3HT nanofibers. The Supporting Information is available free of charge on the ACS Publications website at DOI: 10.1021/acs.jpcc.5b05191.

## AUTHOR INFORMATION

### Corresponding Author

*E-mail jkgrey@unm.edu (J.K.G.).

### Notes

The authors declare no competing financial interest.

## ACKNOWLEDGMENTS

J.K.G. acknowledges financial support from the National Science Foundation (CHE-0955242). M.L.K. acknowledges financial support from the National Science Foundation through Grants CHE-1301142 and IIA-1301346.

## REFERENCES

(1) Furukawa, Y. Electronic Absorption and Vibrational Spectroscopies of Conjugated Conducting Polymers. *J. Phys. Chem.* **1996**, *100*, 15644−15653.

(2) Heeger, A. J. Semiconducting and Metallic Polymers: The Fourth Generation of Polymeric Materials. *J. Phys. Chem. B* **2001**, *105*, 8475−8491.

(3) Luessem, B.; Riede, M.; Leo, K. Doping of Organic Semiconductors. *Phys. Status Solidi A* **2013**, *210*, 9−43.

(4) Pfeiffer, M.; Leo, K.; Zhou, X.; Huang, J. S.; Hofmann, M.; Werner, A.; Blochwitz-Nimoth, J. Doped Organic Semiconductors. Physics and Application in Light Emitting Diodes. *Org. Electron.* **2003**, *4*, 89−103.

(5) Walzer, K.; Maennig, B.; Pfeiffer, M.; Leo, K. Highly Efficient Organic Devices Based on Electrically Doped Transport Layers. *Chem. Rev.* **2007**, *107*, 1233−1271.

(6) Yim, K.-H.; Whiting, G. L.; Murphy, C. E.; Halls, J. J. M.; Burroughes, J. H.; Friend, R. H.; Kim, J.-S. Controlling Electrical Properties of Conjugated Polymers Via a Solution-Based P-Type Doping. *Adv. Mater.* **2008**, *20*, 3319−3324.



DOI: 10.1021/acs.jpcc.5b05191
*J. Phys. Chem. C* 2015, 119, 16396−16402

(7) Chen, J.; Heeger, A. J. In Situ Electron Spin Resonance Experiments on Polyacetylene During Electrochemical Doping. *Synth. Met.* **1988**, *24*, 311−27.
(8) Pingel, P.; Neher, D. Comprehensive Picture of P-Type Doping of P3HT with the Molecular Acceptor F4TCNQ. *Phys. Rev. B: Condens. Matter Mater. Phys.* **2013**, *87*, 115209.
(9) Zhang, Y.; Blom, P. W. M. Enhancement of the Hole Injection into Regioregular Poly(3-Hexylthiophene) by Molecular Doping. *Appl. Phys. Lett.* **2010**, *97*, 083303−3.
(10) Zhang, Y.; de Boer, B.; Blom, P. W. M. Controllable Molecular Doping and Charge Transport in Solution-Processed Polymer Semiconducting Layers. *Adv. Funct. Mater.* **2009**, *19*, 1901−1905.
(11) Aziz, E. F.; Vollmer, A.; Eisebitt, S.; Eberhardt, W.; Pingel, P.; Neher, D.; Koch, N. Localized Charge Transfer in a Molecularly Doped Conducting Polymer. *Adv. Mater.* **2007**, *19*, 3257−3260.
(12) Pingel, P.; Schwarzl, R.; Neher, D. Effect of Molecular P-Doping on Hole Density and Mobility in Poly(3-Hexylthiophene). *Appl. Phys. Lett.* **2012**, *100*, 143303−3.
(13) Zhu, L.; Kim, E.-G.; Yi, Y.; Brédas, J.-L. Charge Transfer in Molecular Complexes with 2,3,5,6-Tetrafluoro-7,7,8,8-Tetracyanoquinodimethane (F4-TCNQ): A Density Functional Theory Study. *Chem. Mater.* **2011**, *23*, 5149−5159.
(14) Mendez, H.; et al. Doping of Organic Semiconductors: Impact of Dopant Strength and Electronic Coupling. *Angew. Chem., Int. Ed.* **2013**, *52*, 7751−7755.
(15) Mityashin, A.; Olivier, Y.; Van Regemorter, T.; Rolin, C.; Verlaak, S.; Martinelli, N. G.; Beljonne, D.; Cornil, J.; Genoe, J.; Heremans, P. Unraveling the Mechanism of Molecular Doping in Organic Semiconductors. *Adv. Mater.* **2012**, *24*, 1535−1539.
(16) Fujita, H.; Yuan, Y.; Michinobu, T. F < Sub > 4</Sub > Tcnq Doping of P3ht:Pcbm Photovoltaic Devices. *J. Photopolym. Sci. Technol.* **2011**, *24*, 311−315.
(17) Loiudice, A.; Rizzo, A.; Biasiucci, M.; Gigli, G. Bulk Heterojunction Versus Diffused Bilayer: The Role of Device Geometry in Solution P-Doped Polymer-Based Solar Cells. *J. Phys. Chem. Lett.* **2012**, *3*, 1908−1915.
(18) Hu, J.; Clark, K. W.; Hayakawa, R.; Li, A.-P.; Wakayama, Y. Enhanced Electrical Conductivity in Poly(3-Hexylthiophene)/Fluorinated Tetracyanoquinodimethane Nanowires Grown with a Porous Alumina Template. *Langmuir* **2013**, *29*, 7266.
(19) Duong, D. T.; Phan, H.; Hanifi, D.; Jo, P. S.; Nguyen, T.-Q.; Salleo, A. Direct Observation of Doping Sites in Temperature-Controlled, P-Doped P3HT Thin Films by Conducting Atomic Force Microscopy. *Adv. Mater.* **2014**, *26*, 6069−6073.
(20) Gao, J.; Niles, E. T.; Grey, J. K. Aggregates Promote Efficient Charge Transfer Doping of Poly(3-Hexylthiophene). *J. Phys. Chem. Lett.* **2013**, *4*, 2953−2957.
(21) Gao, J.; Roehling, J. D.; Li, Y.; Guo, H.; Moule, A. J.; Grey, J. K. The Effect of 2,3,5,6-Tetrafluoro-7,7,8,8-Tetracyanoquinodimethane Charge Transfer Dopants on the Conformation and Aggregation of Poly(3-Hexylthiophene). *J. Mater. Chem. C* **2013**, *1*, 5638−5646.
(22) Brinkmann, M. Structure and Morphology Control in Thin Films of Regioregular Poly(3-Hexylthiophene). *J. Polym. Sci., Part B: Polym. Phys.* **2011**, *49*, 1218−1233.
(23) Sirringhaus, H.; et al. Two-Dimensional Charge Transport in Self-Organized, High-Mobility Conjugated Polymers. *Nature* **1999**, *401*, 685−688.
(24) Osterbacka, R.; An, C. P.; Jiang, X. M.; Vardeny, Z. V. Two-Dimensional Electronic Excitations in Self-Assembled Conjugated Polymer Nanocrystals. *Science* **2000**, *287*, 839−842.
(25) Zerbi, G.; Magnoni, M. C.; Hoogmartens, I.; Kiebooms, R.; Carleer, R.; Vanderzande, D.; Gelan, J. On the Quinoid Structure of Poly(Isothianaphthene). A Vibrational Spectroscopic Study. *Adv. Mater.* **1995**, *7*, 1027−30.
(26) Louarn, G.; Trznadel, M.; Buisson, J. P.; Laska, J.; Pron, A.; Lapkowski, M.; Lefrant, S. Raman Spectroscopic Studies of Regioregular Poly(3-Alkylthiophenes). *J. Phys. Chem.* **1996**, *100*, 12532−12539.
(27) Lapkowski, M.; Pron, A. Electrochemical Oxidation of Poly(3,4-Ethylenedioxythiophene) - "in Situ" Conductivity and Spectroscopic Investigations. *Synth. Met.* **2000**, *110*, 79−83.
(28) Bredas, J. L.; Street, G. B. Polarons, Bipolarons, and Solitons in Conducting Polymers. *Acc. Chem. Res.* **1985**, *18*, 309−15.
(29) Da Silva Pinheiro, C.; E. Silva, G. M. Dynamics of Polarons and Bipolarons with Interchain Coupling in Conjugated Polymers. *Int. J. Quantum Chem.* **2003**, *95*, 153−158.
(30) Niles, E. T.; Roehling, J. D.; Yamagata, H.; Wise, A. J.; Spano, F. C.; Moule, A. J.; Grey, J. K. J-Aggregate Behavior in Poly-3-Hexylthiophene Nanofibers. *J. Phys. Chem. Lett.* **2012**, *3*, 259−263.
(31) Roehling, J. D.; Arslan, I.; Moule, A. J. Controlling Microstructure in Poly(3-Hexylthiophene) Nanofibers. *J. Mater. Chem.* **2012**, *22*, 2498−2506.
(32) Spano, F. C.; Silva, C. H- and J-Aggregate Behavior in Polymeric Semiconductors. *Annu. Rev. Phys. Chem.* **2014**, *65*, 477−500.
(33) Yamagata, H.; Spano, F. C. Interplay between Intrachain and Interchain Interactions in Semiconducting Polymer Assemblies: The Hj-Aggregate Model. *J. Chem. Phys.* **2012**, *136*, 184901/1−184901/14.
(34) Panja, S.; et al. Dianions of 7,7,8,8-Tetracyano-P-Quinodimethane and Perfluorinated Tetracyanoquinodimethane: Information on Excited States from Lifetime Measurements in an Electrostatic Storage Ring and Optical Absorption Spectroscopy. *J. Chem. Phys.* **2007**, *127*, 124301/1−124301/6.
(35) Martin, T. P.; Wise, A. J.; Busby, E.; Gao, J.; Roehling, J. D.; Ford, M. J.; Larsen, D. S.; Moule, A. J.; Grey, J. K. Packing Dependent Electronic Coupling in Single Poly(3-Hexylthiophene) H- and J-Aggregate Nanofibers. *J. Phys. Chem. B* **2013**, *117*, 4478−4487.
(36) Louarn, G.; Buisson, J. P.; Lefrant, S.; Fichou, D. Vibrational Studies of a Series of Alpha -Oligothiophenes as Model Systems of Polythiophene. *J. Phys. Chem.* **1995**, *99*, 11399−404.
(37) Zhao, N.; Noh, Y. Y.; Chang, J. F.; Heeney, M.; McCulloch, I.; Sirringhaus, H. Polaron Localization at Interfaces in High-Mobility Microcrystalline Conjugated Polymers. *Adv. Mater.* **2009**, *21*, 3759−3763.
(38) Tanaka, H.; Hirate, M.; Watanabe, S.; Kuroda, S.-i. Microscopic Signature of Metallic State in Semicrystalline Conjugated Polymers Doped with Fluoroalkylsilane Molecules. *Adv. Mater.* **2014**, *26*, 2376−2383.
(39) Lima, M. P.; E. Silva, G. M. Transition of Polaron to Bipolaron Structure in Conjugated Polymers. *J. Mol. Struct.: THEOCHEM* **2008**, *852*, 15−21.
(40) Lima, M. P.; E. Silva, G. M. Dynamical Evolution of Polaron to Bipolaron in Conjugated Polymers. *Phys. Rev. B: Condens. Matter Mater. Phys.* **2006**, *74*, 224304/1−224304/6.
(41) Koch, N.; Leising, G.; Yu, L. M.; Rajagopal, A.; Pireaux, J. J.; Johnson, R. L. Bipolaron Formation in Para-Sexiphenyl Thin Films Upon Cs Doping. *J. Vac. Sci. Technol., A* **2000**, *18*, 295−298.
(42) Moraes, F.; Davidov, D.; Kobayashi, M.; Chung, T. C.; Chen, J.; Heeger, A. J.; Wudl, F. Doped Poly(Thiophene): Electron Spin Resonance Determination of the Magnetic Susceptibility. *Synth. Met.* **1985**, *10*, 169−79.
(43) Di, B.; Meng, Y.; Wang, Y. D.; Liu, X. J.; An, Z. Formation and Evolution Dynamics of Bipolarons in Conjugated Polymers. *J. Phys. Chem. B* **2011**, *115*, 964−971.
(44) de Oliveira, J. R.; E. Silva, G. M. Interchain Interaction Effects on Polaron-Bipolaron Transition on Conducting Polymers. *J. Mater. Sci.* **2008**, *43*, 585−590.
(45) Zade, S. S.; Bendikov, M. Theoretical Study of Long Oligothiophene Polycations as a Model for Doped Polythiophene. *J. Phys. Chem. C* **2007**, *111*, 10662−10672.
(46) de Brito, A. N.; E. Silva, M. Dynamic Interaction between Polarons and Torsional Vibrations in Conjugated Polymers. *Int. J. Quantum Chem.* **2005**, *103*, 604−609.
(47) Bubnova, O.; et al. Semi-Metallic Polymers. *Nat. Mater.* **2014**, *13*, 190−194.


DOI: 10.1021/acs.jpcc.5b05191
*J. Phys. Chem. C* 2015, 119, 16396−16402